ISSN 0021-8944, Journal of Applied Mechanics and Technical Physics, 2018, Vol. 59, No. 7, pp. 1279–1287. © Pleiades Publishing, Ltd., 2018.
Original Russian Text © A.S. Teimurazov, R.A. Stepanov, M.K. Verma, S. Barman, A. Kumar, S. Sadhukhan, 2018, published in Vychislitel'naya Mekhanika Sploshnykh Sred, 2017, Vol. 10, No. 4, pp. 474–483.

Direct Numerical Simulation of Homogeneous Isotropic Helical Turbulence with the TARANG Code

A. S. Teimurazov[a,*], R. A. Stepanov[a,], M. K. Verma[b,***], S. Barman[b,****], A. Kumar[b,*****], and S. Sadhukhan[b,******]**

[a] *Institute of Continuous Media Mechanics, Russian Academy of Sciences, Ural Branch, ul. Akademika Koroleva 1, Perm, 614013 Russia*

[b] *Department of Physics, Indian Institute of Technology, Kanpur, India*

**e-mail: tas@icmm.ru*

***e-mail: rodion@icmm.ru*

****e-mail: mkv@iitk.ac.in*

*****e-mail: sbarman@iitk.ac.in*

******e-mail: abhishek.kir@gmail.com*

*******e-mail: shubhasports@gmail.com*

Received December 01, 2017; in final form, December 30, 2017

Abstract—The problem of taking into account the influence of turbulence comes up while solving both fundamental questions of geo- and astrophysics and applied problems arising in the development of new engineering solutions. Difficulties in applying the standard propositions of the theory appear when considering flows with a special spatial structure, for example, helical flows. The flow helicity determines the topology of vortices and is conserved in the process of energy transfer in a turbulent flow. In this paper we suggest an approach for numerical simulation of homogeneous isotropic helical turbulence aimed at detecting characteristic signatures of the inertial range and finding the distributions of the spectral energy and helicity densities. In this approach we use the TARANG code designed to numerically solve various problems of fluid dynamics in the regime of a developed turbulent flow and to study hydrodynamic instability phenomena of a different physical nature (thermal convection, advection of passive and active scalars, magnetohydrodynamics, and the influence of Coriolis forces). TARANG is an open source code written in the object-oriented C++ language with a high efficiency of computation on multiprocessor computers. Particular attention in the paper is given to the application of the tool kit from the package to analyze the solutions obtained. The spectral distributions and fluxes of energy and helicity have been computed for Reynolds numbers of 5700 and 14 000 on 512^3 and 1024^3 grids, respectively. We have checked whether the $-5/3$ spectral law is realizable and estimated the universal Kolmogorov and Batchelor constants in the inertial range. An analysis of the energy and helicity transfer functions between the selected scales (shell-to-shell transfer) shows a significant contribution of nonlocal interactions to the cascade process.

Key words: helical turbulence, direct numerical simulation, pseudospectral method, TARANG code.

DOI: 10.1134/S0021894418070131

1. INTRODUCTION

The description of turbulent flows of a continuous medium remains one of the most acute modern problems of gas, fluid, and plasma mechanics. The problems being solved concern both fundamental questions of geo- and astrophysics and applied problems arising in the development of new technologies. The fundamentals of the theory of turbulence were developed in the past century, and the $-5/3$ spectral law formulated by Kolmogorov [1] primarily refers to them. Full-scale experimental studies of turbulent fluid and gas flows near various surfaces or in volumes were carried out at the same time [2]. The derived phenomenological relations for mean fields, which are in satisfactory agreement with experiments, allow many engineering problems to be solved even now. However, the ever-increasing complication of technology and the need for parameter optimization require more accurate solutions. The intensive development of computing technology in the last decades has brought computer simulation to the fore as the main research tool.

Widespread software packages for applied problems allow the turbulent nature of motion to be taken into account. As a rule, the problem is not solved in all details, but some model of turbulence is used. This approach works very well in simple cases. Depending on the turbulence generation method, the flow can be characterized by helicity, which determines the topology of vortices and is conserved in the process of energy transfer in a turbulent flow. Topical questions related to the helicity have attracted attention of many researchers, while experimental and theoretical results are published in the most cited multidisciplinary journals [3, 4]. In problems with a complex geometry or in the presence of several active fields (convection, magnetohydrodynamics, active chemistry), a verification of the computations is required to answer the question of whether a particular model of turbulence is applicable in each specific case. The necessary information can be obtained with the help of an experiment (which, as a rule, is very expensive or even unfeasible) or one can resort to complete (direct) numerical simulation. In the latter case, the success of the study will depend on the computational efficiency of the method and the flexibility of the package in terms of the problem statement.

At present, the methods for direct numerical simulation are being continuously developed. Most of the codes are based on algorithms using finite elements, finite differences, finite volumes or spectral transformations [5]. A lot of works whose results are not discussed here are devoted to a comparative analysis of the techniques with their application.

The goal of this paper to demonstrate the capabilities of direct numerical simulation of turbulence with TARANG code [6]. Among the advantages of the package are: a high parallelization efficiency; free package; a continuous update by an actively working group of researchers; transparent configuration for easy learning and applications. In this paper we describe the characteristic features of the TARANG and demonstrate its use by studying the spectral distributions and fluxes of energy and helicity in homogeneous and isotropic turbulence generated in a cubic region with periodic boundaries as an example. We show the $-5/3$ spectral law to be realizable and the possibility of determining the universal Kolmogorov and Batchelor constants in the inertial range of helical turbulence scales.

2. THE TARANG COMPUTATIONAL CODE AND THE PSEUDOSPECTRAL METHOD

TARANG (in translation from Sanskrit means "waves") is a software package designed to solve various problems of fluid dynamics in the turbulent regime and to study hydrodynamic instability phenomena of different nature. This modular code written in the object-oriented C++ programming language implements parallel computations for launching on multiprocessor computers. It allows incompressible fluid flows to be simulated in various configurations: the motion of a fluid under the action of an external force, Rayleigh–Bénard convection, turbulence with passive and active scalars, magnetohydrodynamics, turbulence in rotating systems, etc. TARANG is software with an open source code and can be downloaded from the website http://turbulencehub.org.

In this paper we show the capabilities of the TARANG code for direct numerical simulation of incompressible hydrodynamic flows described by the Navier–Stokes equations:

$$\frac{\partial \mathbf{u}}{\partial t} + \mathbf{u}\cdot\nabla\mathbf{u} = -\nabla P + \nu\nabla^2\mathbf{u} + \mathbf{F}, \tag{1}$$

$$\nabla\cdot\mathbf{u} = 0. \tag{2}$$

Here, $\mathbf{u}$ is the velocity vector, P is the pressure (divided by density), ν is the kinematic viscosity, $\mathbf{F}$ is the vector field of the external force density acting on the fluid. Equations (1) and (2) are solved using a pseudospectral method. For this purpose, they are written in Fourier space as

$$(\partial_t + \nu k^2)\hat{u}_j = -ik_l\widehat{u_l u_j} - ik_j\hat{P} + \hat{F}_j, \tag{3}$$

$$k_j\hat{u}_j = 0; \tag{4}$$

here, i is the imaginary unit and k_j are the wave vector components. The symbol "$\hat{}$" denotes the Fourier transform of the field. These equations are integrated over time using a Runge–Kutta scheme with an adaptive step. The nonlinear term $\widehat{u_l u_j}$ in spectral space is a convolution; finding it requires performing $O(N^6)$ operations on floating-point numbers on a computational grid with a size N^3. To save computer resources when calculating $\widehat{u_l u_j}$, the inverse Fourier transform is performed for $\hat{u}_j$ and the product $u_l u_j$ is determined in physical space, whereupon the Fourier transform is found for this product (see Fig. 1).

When using the fast Fourier transform (FFT), only $O(N^3\log(N^3))$ operations are required to calculate the nonlinear term according to the described scheme [7]. Since multiplication needs to be performed in

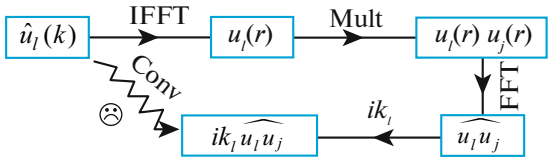

Fig. 1. Schematic diagram for computing the nonlinear term $\widehat{\mathbf{u}\cdot\nabla\mathbf{u}}$ in the pseudospectral method.

physical space to calculate the nonlinear term, this method is called pseudospectral. Multiple transforms of the nonlinear term from Fourier space to physical one and back result in aliasing effect, which leads to the accumulation of errors that can be gotten rid of by filling only 2/3 of the array of variables in each direction [7, 8].

TARANG possesses a wide set of capabilities [6] to employ external forces that allows helical turbulence with controllable characteristics to be generated.

3. EXTERNAL FORCE PARAMETRIZATION

The injection of energy and helicity into the system is provided by the action of a specified force $\mathbf{F}(\mathbf{k})$ (which generally also depends on time). The properties of the force will influence the nature of the turbulence being realized. The specific choice of $\mathbf{F}(\mathbf{k})$ parametrization plays an important role and largely determines the research possibilities. The force usually acts only on the system's large scales so that the flux remains constant in the inertial range. Any force (including a random one) can serve as a source of energy due to the autocorrelation property [9]. For the injection of helicity the force must be such that the real part of the expression $\mathbf{F}(\mathbf{k})\cdot(\mathbf{k}\times\mathbf{F}^*(\mathbf{k}))$ has a constant sign. The actual injection of energy and helicity will be determined by the velocity field and, hence, will be poorly controllable. The constancy of the rate of change in energy and helicity is provided by introducing the dependence of the force on velocity $\mathbf{u}(\mathbf{k})$. The behavior of this dependence can be both deterministic and random. Both cases are implemented in the TARANG.

Below we give an example of the parametrization of a deterministic force that provides a specified injection rate of energy ε_E and helicity ε_H into the range of scales $k_0^F \le |\mathbf{k}| \le k_1^F$, which is specified by two wave numbers k_0^F and k_1^F. At a given time the force is represented as a linear combination of the velocity $\mathbf{u}$ and vorticity $\boldsymbol{\omega} = \nabla\times\mathbf{u}$:

$$\mathbf{F}(\mathbf{k}) = \alpha\mathbf{u}(\mathbf{k}) + \beta\boldsymbol{\omega}(\mathbf{k}), \tag{5}$$

where α and β are indeterminate dimensional parameters. Given the energy and helicity expressions for the mode $\mathbf{u}(\mathbf{k})$:

$$E(\mathbf{k}) = \frac{1}{2}|\mathbf{u}(\mathbf{k})|^2, \quad H(\mathbf{k}) = \frac{1}{2}\Re\{\mathbf{u}^*(\mathbf{k})\cdot\boldsymbol{\omega}(\mathbf{k})\}, \tag{6}$$

the energy injection rate into the modes located in the range of forcing scales will be

$$\varepsilon_E = \sum_{k_0^F\le|\mathbf{k}|\le k_1^F}\Re\{\mathbf{F}(\mathbf{k})\cdot\mathbf{u}^*(\mathbf{k})\} = \sum_{k_0^F\le|\mathbf{k}|\le k_1^F}\alpha|\mathbf{u}(\mathbf{k})|^2 + \beta\Re\{\mathbf{u}^*(\mathbf{k})\cdot\boldsymbol{\omega}(\mathbf{k})\} = 2\alpha E_F + 2\beta H_F, \tag{7}$$

where E_F and H_F are the total energy and helicity of the flow on the forcing scales. The helicity injection rate is calculated in a similar way:

$$\varepsilon_H = \frac{1}{2}\sum_{k_0^F\le|\mathbf{k}|\le k_1^F}\Re\{\mathbf{F}(\mathbf{k})\cdot\boldsymbol{\omega}^*(\mathbf{k}) + \mathbf{u}(\mathbf{k})\cdot(-i\mathbf{k}\times\mathbf{F}(\mathbf{k}))\} = 2\alpha H_F + 2\beta W_F, \tag{8}$$

where $W_F = \sum k^2 E(\mathbf{k})$ denotes the enstrophy of the forcing scales. By solving Eqs. (7) and (8), we can find the coefficients α and β:

$$\alpha = \frac{1}{2}\frac{W_F\varepsilon_E - H_F\varepsilon_H}{E_F W_F - H_F^2}, \quad \beta = \frac{1}{2}\frac{E_F\varepsilon_H - H_F\varepsilon_E}{E_F W_F - H_F^2}. \tag{9}$$

Note that in view of the constraint on the helicity $H(\mathbf{k}) \le kE(\mathbf{k})$, the denominator in (9) satisfies the condition $E_F W_F - H_F^2 \ge 0$ (the exact equality never holds in practice). Expressions (9) can also be derived for

variable values of $\varepsilon_E(k)$ and $\varepsilon_H(k)$. Turbulence with a spectrally distributed source of helicity can be simulated in this case as well [10].

4. PROCESSING OF THE NUMERICAL SOLUTION (POST-PROCESSING)

The direct numerical integration of (3) is a complex and resource intensive. However, the success of the study of turbulent flows depends on the capabilities of post-processing. Determining reliable values of the turbulent characteristics takes a long time for numerical simulations (hundreds of realizations) to achieve the necessary statistical reliability. Since it is impossible to save the results in full, the research strategy and the post-processing procedures should be chosen in advance.

A universally accepted approach in studying turbulent flows is to construct the spectrum—the spectral density distribution. The detection of a segment of the spectrum with $-5/3$ law is generally believed to be a proof of the existence of an inertial range with a turbulent cascade. Note however that this is not always the case. Various turbulent energy and helicity transfer mechanisms can be responsible for the emergence of a particular spectral distribution. The spectral energy and helicity fluxes provide validation of a model. Despite the obviousness of this assertion, such an analysis is performed quite rarely. Apparently, this is mainly explained by the additional difficulty in calculating the third moments of the velocity field that determine the spectral fluxes. TARANG code includes the necessary set of numerical post-processing procedures. Below we give mathematical formulations of the main computational algorithms.

The problem of finding the spectral density lies in the necessity of numerical integration of a function specified on a Cartesian grid over a sphere in Fourier space. In practice Fourier space is broken down into spherical shells S_n with thickness Δk:

$$S_n = \{\mathbf{k}' \in \mathbb{R}^3 / n\Delta k < |\mathbf{k}'| \le (n+1)\Delta k\}, \tag{10}$$

and the spectral energy density in a shell E_n is then assumed to be approximately equal to the sum of the energies of the Fourier modes in the shell S_n divided by Δk. However, this procedure leads to strong beats, especially in the long-wavelength part of the spectrum [11]. A more accurate result is obtained if the energies of the modes are summed with their relative weights

$$E_n = \frac{4\pi}{M_n} \sum_{\mathbf{k}' \in S_n} \hat{E}(\mathbf{k}') |\mathbf{k}'|^2, \tag{11}$$

where M_n is the number of modes belonging to the shell S_n. The wave number associated with S_n should be calculated as an average:

$$k_n = \frac{1}{M_n} \sum_{\mathbf{k}' \in S_n} |\mathbf{k}'|. \tag{12}$$

This relatively simple solution of the problem proposed in [11] has so far been used only in a few papers [12, 13], but it allowed the determination of spectral characteristics to be improved qualitatively.

The spectral fluxes are calculated using an expressions for the spectral transfer function T from mode $\mathbf{u}(\mathbf{p})$ to mode $\mathbf{u}(\mathbf{k})$ with the involvement of mode $\mathbf{u}(\mathbf{q})$, which together form a triad $\mathbf{k} + \mathbf{p} + \mathbf{q} = 0$ [14]. For the energy transfer we have the expression

$$T_E(\mathbf{k}|\mathbf{p}|\mathbf{q}) = \Re\{\langle \mathbf{u}(\mathbf{q}), \boldsymbol{\omega}(\mathbf{p}), \mathbf{u}(\mathbf{k}) \rangle\}, \tag{13}$$

where $\boldsymbol{\omega}(\mathbf{p}) = i\mathbf{p} \times \mathbf{u}(\mathbf{p})$ is the vorticity for the wave vector $\mathbf{p}$ and the brackets $\langle ... \rangle$ denote the mixed product of vectors. The total spectral flux $\Pi(k_0)$ on a scale with a wave number k_0 is then calculated as

$$\Pi(k_0) = \sum_{k > k_0} \sum_{p \le k_0} T(\mathbf{k}|\mathbf{p}|\mathbf{q}). \tag{14}$$

This corresponds to the enumeration of all possible triads, which is unfeasible in practice even for coarse grids. One way to overcome this restriction is that the convolution of the Fourier modes should be found in physical space. The energy transfer function from shell m to shell n is then calculated as follows:

$$Q_E(n,m) = \Re\left\{ \sum_{\mathbf{k} \in S_n} \left[\sum_{\mathbf{p} \in S_m} \mathbf{u}(\mathbf{q}) \times \boldsymbol{\omega}_m(\mathbf{p}) + \mathbf{u}(\mathbf{p}) \times \boldsymbol{\omega}_m(\mathbf{q}) \right] \cdot \mathbf{u}_n(\mathbf{k}) \right\} = \Re\left\{ \sum_{\mathbf{k} \in S_n} \mathbf{N}(\mathbf{k}) \cdot \mathbf{u}_n(\mathbf{k}) \right\}, \tag{15}$$

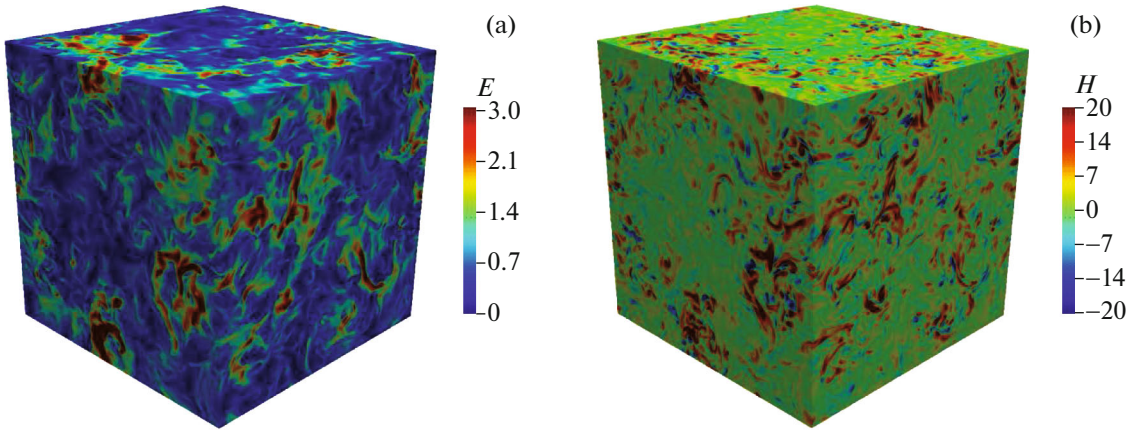

Fig. 2. The instantaneous fields obtained in our computations for the 512^3 grid: (a) the energy distribution; (b) the helicity distribution (the color illustration is accessible in the online version)

where

$$\mathbf{u}_n(\mathbf{k}) = \begin{cases} \mathbf{u}(\mathbf{k}), & \mathbf{k} \in S_n, \\ 0, & \mathbf{k} \notin S_n. \end{cases} \tag{16}$$

In this case, $\mathbf{N}(\mathbf{k})$ is calculated in physical space, while the sum $\mathbf{N}(\mathbf{k}) \cdot \mathbf{u}_n(\mathbf{k})$ is calculated in Fourier space. The total spectral flux through shell n is found by summation:

$$\Pi(n) = \sum_{l>n} \sum_{m \le n} Q(l,m). \tag{17}$$

5. RESULTS

The computational domain was a cube with a side of 2π with periodic boundary conditions. In all our computations the energy was injected in the range of scales $2 \le k \le 4$, the energy injection rate was fixed at $\varepsilon_E = 0.1$, and ν was chose so as to achieve the maximum Reynolds number at a given grid resolution. The computations were carried out on 512^3 and 1024^3 grids. As the practical experience shows, these are the most optimal variants in the sense that it is quite realistic to carry out such computations on regional supercomputers and, at the same time, there is sufficient resolution to study the peculiarities of cascade processes. For the 512^3 grid the viscosity was $\nu = 10^{-3}$, which corresponded to the Reynolds number $\mathrm{Re} = u_{\mathrm{rms}} L/\nu = 5700$ and the Kolmogorov scale $k_d = (\nu^3/\varepsilon_E)^{-1/4} = 100$. For the 1024^3 grid the viscosity was $\nu = 4 \times 10^{-4}$, and $\mathrm{Re} = 14\,000$ and $k_d = 199$ were reached. We compared the spectral characteristics of turbulence without ($\varepsilon_H = 0$) and with helicity at $\varepsilon_H = 0.35$. The averaging time in all our computations was at least 25 time units.

The instantaneous spatial energy and helicity distributions are presented in Fig. 2. It can be seen that large-scale structures are present in the energy distribution, which corresponds well to the forcing range. In the helicity distribution structures with positive and negative signs alternate, but, on average, the positive helicity dominates.

5.1. Code Scalability

The computations were carried out on two supercomputers: Triton (Institute of Continuous Media Mechanics, the Siberian Branch of the Russian Academy of Sciences, Perm) and Shaheen II (King Abdullah University of Science and Technology, Saudi Arabia). The Triton supercomputers with a peak performance of 23.1 Tflops is based on Intel Xeon E5450 (Harpertown generation, 256 processor cores) and Intel Xeon E5-2690v4 (Broadwell generation, 448 processor cores) processors with an InfiniBand FDR interconnect. The Shaheen II supercomputer is based on Intel Xeon E5-2698v3 (Haswell generation, 196608 processor cores) processors with an Aries interconnect and has a peak performance of 7.2 Pflops.

Figure 3 demonstrates the scalability of the TARANG code in our computations on the 512^3 and 1024^3 grids. On the 512^3 grid on Shaheen II, the speedup of the computations on 16 384 processors is a fac-

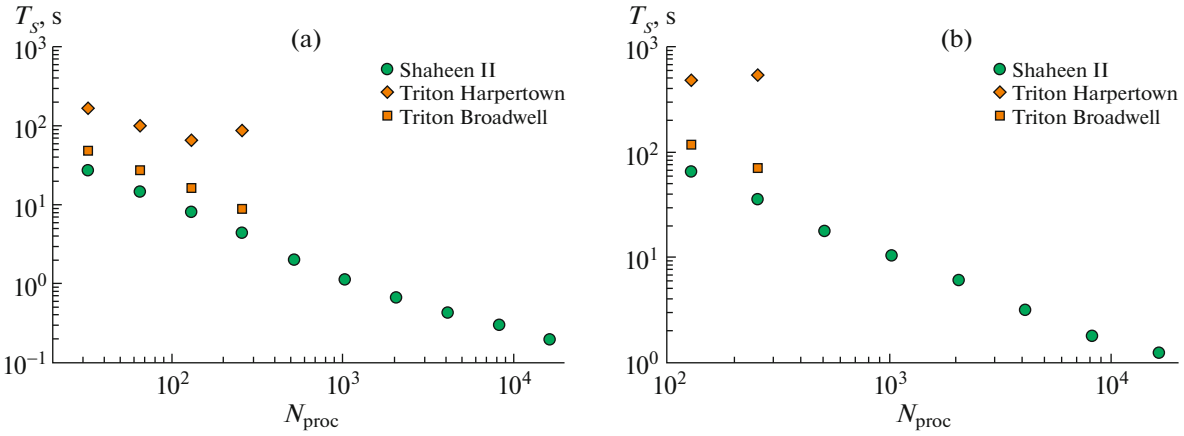

Fig. 3. Execution time of one computational step T_S versus number of processors N_{proc}. (a) The 512^3 grid; (b) the 1024^3 grid.

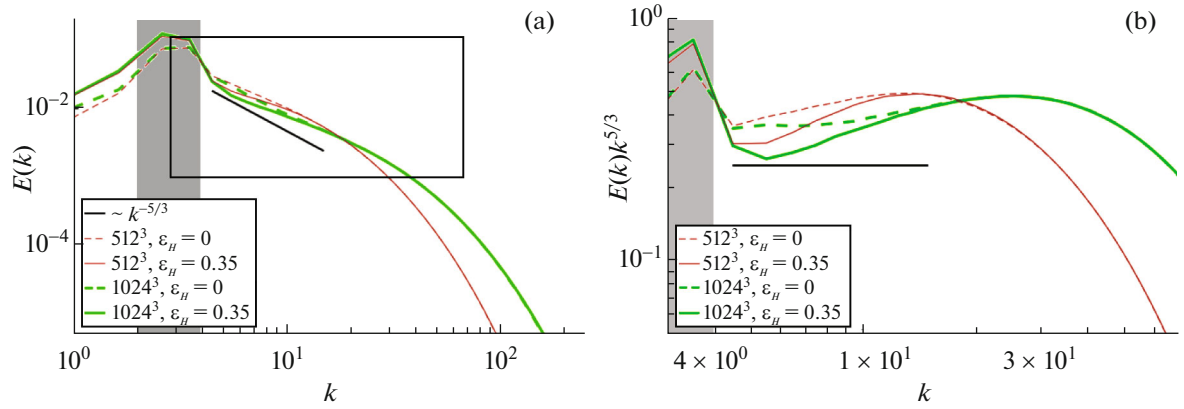

Fig. 4. (a) Comparison of the energy spectra for helical and nonhelical flows computed on the 512^3 and 1024^3 grids; (b) the energy spectrum compensated by $k^{5/3}$ on an enlarged scale (see the zone marked on panel (a) by the rectangle); the energy and helicity injection range is indicated by the gray color.

tor of 138 compared to the computations on 32 processors. When using the Harpertown processors of the Triton cluster, a speedup by a factor of 2.6 when passing from 32 to 128 processors is observed. However, when 256 processors are enabled, the execution time of one computational step increases, which can be explained by the peculiarities of the data exchange network between cluster segments. The application of higher-performance Broadwell-generation processors on the Triton cluster allows a speedup by a factor of 5.4 to be achieved when passing from 32 to 256 processors. The same trends are also traceable in our computations on the 1024^3 grid. It should be noted that 25 computational time units on the 1024^3 grid correspond to $\approx 10^5$ steps.

5.2. Energy and Helicity Spectra

The representation of the energy spectra shown in Fig. 4a allows to identify the energy injection scales, where the spectrum peaks (highlighted by the gray color), and the dissipation scales, where the spectrum is abruptly cut off. At a higher resolution (on the 1024^3 grid), the inertial range is wider, but the range of scales where the $-5/3$ law holds with a sufficient accuracy cannot be determined. This is feasible only when considering the compensated spectra presented in Fig. 4b. On the 512^3 grid the spectrum begins to rise immediately after the jump at the boundary of the forcing range, this is how the bottleneck effect manifests itself [15], while on the 1024^3 grid there is a horizontal segment up to $k < 10$. The differences between the helical and nonhelical cases are clearly seen in the compensated spectra. In helical turbu-

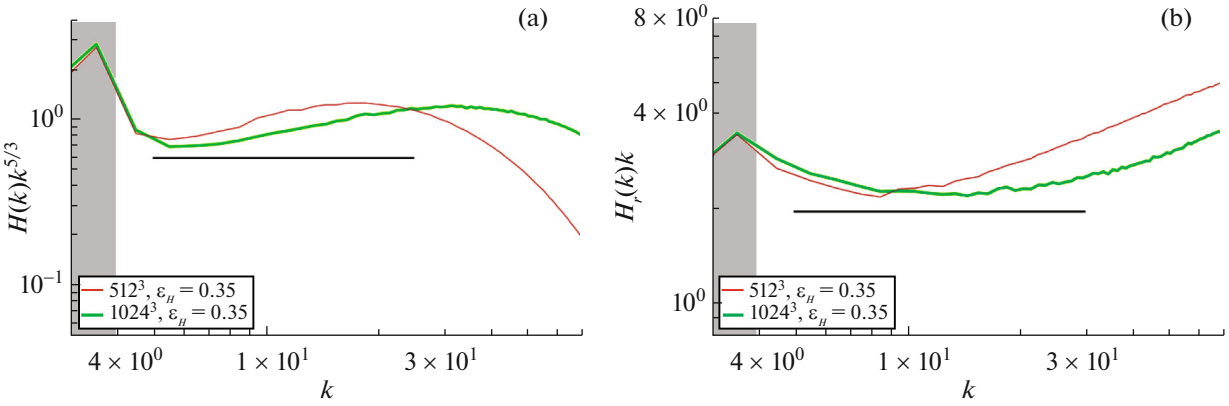

Fig. 5. The helicity spectra compensated by $k^{5/3}$ (a) and the spectra of relative helicity H_r compensated by k (b); the energy and helicity injection range is indicated by the gray color.

lence, the energy level rises on the injection scales and falls in the inertial range of scales. Note that helicity does not change the energy distribution on the dissipative scales.

The classical views of helical turbulence suggests that the helicity introduced into the flow on a large scale must be transferred to small scales as a passive scalar. On the whole, the helicity spectra presented in Fig. 5a correspond to this scenario. In reality, the distributions of relative helicity $H_r(k) = H(k)/(kE(k))$ (Fig. 5b) turn out to be more informative. The law $H_r(k) \sim k^{-1}$, which was used for the compensation, is predicted theoretically. It turns out that the chosen regime of helicity injection is the maximally possible one, because $H_r(k)$ reaches its maximum equal to 1. Note that no horizontal segment is observed on scales $k < 10$. To explain the obtained spectral energy and helicity distributions, we should consider their spectral fluxes presented in the next section.

Estimates for the Kolmogorov constant K_E and the Batchelor constant K_H can be obtained from the energy (Fig. 4) and helicity (Fig. 5) spectra:

$$E(k) = K_E \varepsilon_E^{2/3} k^{-5/3}, \tag{18}$$

$$H(k) = K_H \varepsilon_H \varepsilon_E^{-1/3} k^{-5/3}. \tag{19}$$

It is impossible to obtain such estimates on the 512^3 grid due to the absence of an extended interval corresponding to the $-5/3$ law in the spectra. Therefore, the estimates for the constants were made only for the 1024^3 grid. In the case of nonhelical turbulence, the Kolmogorov constant is $K_E = 1.68 \pm 0.04$ when averaged on the segment $4.5 \le k \le 10.5$, which corresponds to the well-known results [16]. For helical turbulence the $-5/3$ law is not reproduced even for the 1024^3 grid. The estimates of $K_E = 1.4 \pm 0.1$ and $K_H = 1.1 \pm 0.1$ found for this case may be deemed effective. The lower value of K_E can be explained by a decrease in the fraction of the spectral energy flux provided by local interactions. For a phenomenological description of this situation the representation (18) must be corrected, for example, by substituting the local fraction Π_E for ε_E.

5.3. Spectral Energy and Helicity Fluxes

The spectral energy and helicity fluxes presented in Fig. 6 allow us to estimate whether the necessary condition for the realization of the $-5/3$ law or, more specifically, the presence a range of scales with a constant flux, is satisfied. The significant difference between the fluxes obtained on different grids is a strong argument for performing computations on the 1024^3grid. The coincidence of the actual energy and helicity fluxes with the specified values of ε_E and ε_H suggests a good parametrization of the force.

Let us consider the questions of spectral transfer in more detail using the spectral transfer function between two shells $Q(n, m)$ (shell-to-shell transfer). In this paper we used the split of Fourier space into

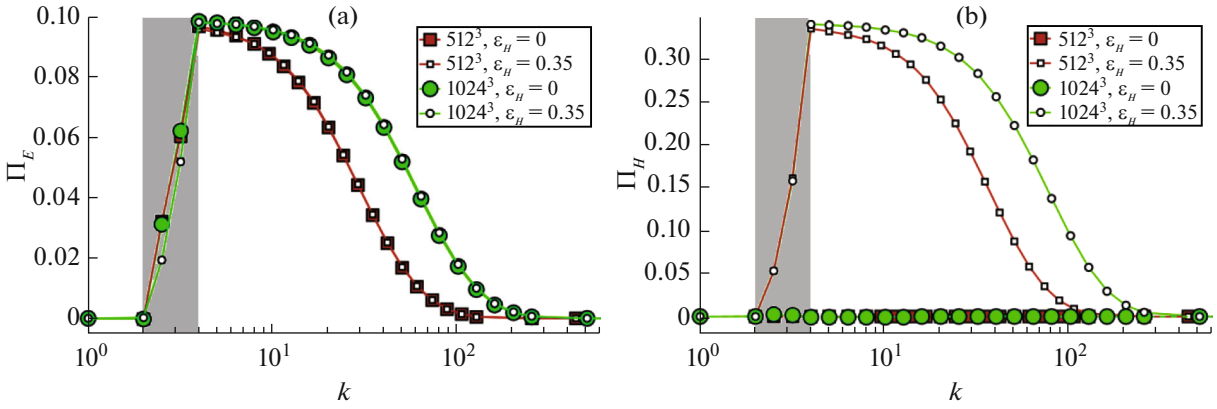

Fig. 6. The spectral fluxes for helical and nonhelical computations on different grids: (a) the energy flux, (b) the helicity flux; the energy and helicity injection range is indicated by the gray color.

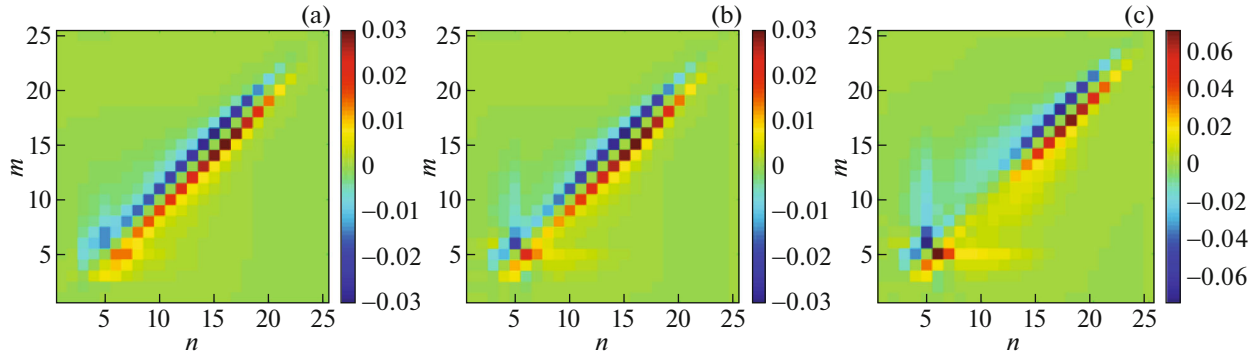

Fig. 7. The spectral shell-to-shell transfer of energy and helicity for the 1024^3 grid. (a) Q_E at $\varepsilon_H = 0$; (b) Q_E at $\varepsilon_H = 0.35$; (c) Q_H at $\varepsilon_H = 0.35$

25 shells as follows: $k_n = \{0,1,2^{n/3},...,512\}$. The representation of $Q(n,m)$ for the 1024^3 grid shown in Fig. 7 allows the cascade process to be analyzed in detail. The predominance of the shell-to-shell energy transfer between adjacent shells almost in the entire range of wave numbers suggests the realization of a direct cascade through local interactions ($Q_E(n,n-1) > 0$ and $Q_E(n,n+1) < 0$), which provide ~30% of the total spectra energy flux. In the case of helical turbulence (Fig. 7b), the local energy transfer is suppressed in shells with numbers $5 < n < 9$, whose contribution drops to ≈10%, and the spectral flux is realized through the nonlocal transfer from the shell with $n = 5$ to approximately up to the 12th shell. The nonlocal shell-to-shell transfer, which is seen as horizontal and vertical streaks, is even more pronounced for helicity (Fig. 7c). The diagonal (local transfer) in Q_H is absent starting from the forcing scale ($n = 5$) to $n = 12$. The local helicity transfer appears from $n = 12$. The distribution $H_r(k) \sim k^{-1}$ is observed in this part of the spectrum (see Fig. 5b).

6. CONCLUSIONS

We considered the spectral distributions and spectral fluxes of energy and helicity in homogeneous isotropic helical turbulence. The problem was solved by direct numerical simulation using TARANG—an open source code. The capabilities of the code, especially with regard to a post-processing analysis, were described. The computational procedures for finding the functions of the spectral densities and spectral exchange of energy and helicity between various scales were described in detail. We showed that the proposed model of an external turbulent force allows one to accurately control the injection rate of energy and helicity in order to achieve the maximum possible degree of helicity when applied in practice. We found that turn from a 512^3 to a 1024^3 grid leads to the appearance of the inertial range with the $-5/3$ law. A detailed analysis

of the cascade process of helical turbulence with the application of the spectral shell-to-shell transfer revealed a significant enhancement of the nonlocal energy and helicity exchange between various scales in the inertial range. Estimates of the universal Kolmogorov and Batchelor constants in the inertial range of scales were given for each of the cases considered.

ACKNOWLEDGMENTS

This work was financially supported by the Russian Science Foundation (project no. 16-41-02012) and the Ministry of Science and Technologies of India (grant INT/RUS/RSF/3). For our computations we used resources of the Triton (Institute of Continuous Media Mechanics, the Ural Branch of the Russian Academy of Sciences) and Shaheen II (Supercomputer Laboratory, KAUST, Saudi Arabia) supercomputers under support of the K1052 project.

REFERENCES

1. Kolmogorov, A.N., The local structure of turbulence in incompressible viscous fluid for very large Reynolds numbers, *Dokl. Akad. Nauk SSSR,* 1941, vol. 30, no. 4, pp. 301–304.
2. Schlichting, H., *Boundary-Layer Theory,* New York: McGraw-Hill, 1955.
3. Scheeler, M.W., van Rees, W.M., Kedia, H., Kleckner, D., and Irvine, W.T.M., Complete measurement of helicity and its dynamics in vortex tubes, *Science (Washington, DC, U. S.),* 2017, vol. 357, no. 6350, pp. 487–490. http://dx.doi.org/ doi 10.1126/science.aam6897
4. Moffatt, H.K., Helicity-invariant even in a viscous fluid, *Science (Washington, DC, U. S.),* 2017, vol. 357, no. 6350, pp. 448–449. http://dx.doi.org/ doi 10.1126/science.aao1428
5. Ferziger, J.H. and Peric, M., *Computational Methods for Fluid Dynamics,* Berlin: Springer, 2002.
6. Verma, M.K., Chatterjee, A.G., Reddy, S., Yadav, R.K., Paul, S., Chandra, M., and Samtaney, R., Benchmarking and scaling studies of pseudospectral code Tarang for turbulence simulations, *Pramana-J. Phys.,* 2013, vol. 81, no. 4, pp. 617–629. http://dx.doi.org/ doi 10.1007/s12043-013-0594-4
7. Canuto, C., Hussaini, M.Y., Quarteroni, A., and Zhang, T.A., *Spectral Methods in Fluid Turbulence,* Berlin: Springer, 1988.
8. Boyd, J.P., *Chebyshev and Fourier Spectral Methods,* 2nd ed., New York: Dover, 2001.
9. Alvelius, K., Random forcing of three-dimensional homogeneous turbulence, *Phys. Fluids,* 1999, vol. 11, no. 7, pp. 1880–1889. http://dx.doi.org/ doi 10.1063/1.870050
10. Kessar, M., Plunian, F., Stepanov, R., and Balarac, G., Non-Kolmogorov cascade of helicity-driven turbulence, *Phys. Rev. E,* 2015, vol. 92, p. 031004(R). http://dx.doi.org/ doi 10.1103/PhysRevE.92.031004
11. Stepanov, R., Plunian, F., Kessar, M., and Balarac, G., Systematic bias in the calculation of spectral density from a three-dimensional spatial grid, *Phys. Rev. E,* 2014, vol. 90, no. 5, p. 053309. http://dx.doi.org/ doi 10.1103/PhysRevE.90.053309
12. McKay, M.E., Linkmann, M., Clark, D., Chalupa, A.A., and Berera, A., Comparison of forcing functions in magnetohydrodynamics, *Phys. Rev. Fluids,* 2017, vol. 2, no. 11, p. 114604. http://dx.doi.org/ doi 10.1103/PhysRevFluids.2.114604
13. Stepanov, R., Teimurazov, A., Titov, V., Verma, M.K., Barman, S., Kumar, A., and Plunian, F., Direct numerical simulation of helical magnetohydrodynamic turbulence with TARANG code, 2017 Ivannikov ISPRAS Open Conference (ISPRAS), Moscow, 2017, pp. 90–96. http://dx.doi.org/ doi 10.1109/ISPRAS.2017.00022
14. Verma, M.K., Statistical theory of magnetohydrodynamic turbulence: recent results, *Phys. Rep.,* 2004, vol. 401, no. 5, pp. 229–380. http://dx.doi.org/ doi 10.1016/j.physrep.2004.07.007
15. Donzis, D.R. and Sreenivasan, A.K., The bottleneck effect and the Kolmogorov constant in isotropic turbulence, *J. Fluid Mech.,* 2010, vol. 657, pp. 171–188. http://dx.doi.org/ doi 10.1017/S0022112010001400
16. Yeung, P.K. and Zhou, Y., Universality of the Kolmogorov constant in numerical simulations of turbulence, *Phys. Rev. E,* 1997, vol. 56, no. 2, pp. 1746–1752. http://dx.doi.org/ doi 10.1103/PhysRevE.56.1746

Translated by V. Astakhov